Final Report Year 1

Portable Chemical Agent Detection System: Differential Reflectometer and Light Scattering Approaches

Submitted to Dr. Chris Palmer
Department of Chemistry
University of Montana
Bozeman, MT

Submitted by
Paul H. Holloway, Rolf Hummel and Mark Davidson
Department of Materials Science and Engineering and MICROFABRITECH
University of Florida
Gainesville, FL 32611-6400

February 15, 2005

1st ANNUAL REPORT

MARCH 2003 – SEPTEMBER 2004

Portable Chemical Agent Detection System

DAAD19-03-2-0004

University of Montana

Christopher P. Palmer and Michael D. DeGrandpre, PIs

Introduction

Detecting chemical agents and energetic materials quickly at very low concentration levels and identifying them accurately is highly desirable. This report describes the results of the first year of a program to develop fundamental knowledge and technology for ultimate use in a portable optical sensor for chemical agents and explosives, and initial efforts to develop a prototype instrument based on sensor technology developed as part of the project. Development of the sensor involves the evaluation and development of several very sensitive spectroscopic techniques based upon luminescence spectroscopy. A novel waveguiding fused silica capillary tubing, photofragmentation coupled with luminol chemiluminescence, and direct photoluminescence spectroscopy have been utilized and micro- and macro-mechanical systems for sample collection are have been evaluated.

FOCAP technology

The detection of organophosphate chemical warfare agents and energetic materials is being developed based on the use of fluorescence spectroscopy and novel waveguiding fused silica capillary tubing, so named Fiber Optic Capillaries (FOCAP). The novel capillary tubing is doped on the outer wall so that light is guided within the wall. Optical detection is achieved through an evanescent field interaction with an absorbing medium at the inner wall interface. Evanescent wave absorption spectroscopy is well understood and has been used in various sensing techniques.[1] Sensors based a similar approach where the selective chemistry was immobilized at the tip of a fiber optic have been developed previously, and have been used to detect pesticides, explosives, and chemical weapons.[2] Some specific examples include the detection of the pesticides carbaryl and dichlorvos by immobilizing cholinesterase on the surface

---

1 Harrick, N.J. Internal Reflection Spectroscopy, Harrick Scientific Corporation: New York, (1979). Ruddy, V.; MacCraith, B. D.; Murphy, J. A. Journal of Applied Physics (1990), 67(10), 6070-4. Wolfbeis, Otto S. Trends in Analytical Chemistry (1996), 15(6), 225-232. Messica, A.; Greenstein, A.; Katzir A. Applied Optics (1996), 35(13) 2274-2284.

2 Wolfbeis, Otto S. Trends in Analytical Chemistry (1996), 15(6), 225-232. Messica, A.; Greenstein, A.; Katzir A. Applied Optics (1996), 35(13) 2274-2284. Mueller, Gerhard J. ACS Symp. Ser. (1979), 102, 239-62. Clonis et al. Biosensors & Bioelectronics. 2002. 17, 61-69. Shriver-Lake et al. Analytica Chimica Acta. 1999. 399, 13-20

of a sol-gel layer,[3] a competitive immunoassay on an antibody-coated fiber optic to detect TNT and RDX,[4] and a modified heme to detect a change in fluorescence in the presence of nitric oxide.[5]

Importantly, FOCAP sensors utilize interactions at the chemically modified surface over the length of the waveguide for increased signal. FOCAP sensors thus allow for increased sensitivity compared to other evanescent field devices due to the increased optical path lengths that can be achieved with long (meters) capillary waveguides. FOCAP sensors will also accommodate either gas or liquid samples in a convenient tubular geometry. Because of their relatively recent availability, the optical properties of the light guiding fused silica capillary tubing have not been fully investigated. A thorough assessment of the light guiding properties and fundamental response characteristics of these novel capillaries will aid in optimizing the sensitivity of a chemically modified capillary for chemical warfare agent and explosives detection. Both absorption and fluorescence spectroscopy are being used to evaluate the interaction between the evanescent wave and light absorbing compounds located on the inner wall of these capillary waveguides.

Ultimate applications of the FOCAP sensors will utilize fluorescence-based detection methods due to increased sensitivity compared to absorbance methods. Sensitive and selective chemical reagents will be immobilized on the inner wall of the FOCAP sensor. The chemically modified surfaces will be selective to the target analytes and will provide an enhanced or quenched fluorescent signal in the presence of the target analytes at very low analyte concentrations. The selectivity of the sensor will result from highly specific biochemical or chemical interactions. In the current project, protocols for chemical immobilization and characterization of the immobilized species were investigated.

Light intensity throughput studies

We utilized the University of Montana Core Spectroscopy Facility for the initial stages of FOCAP sensor characterization. This facility has a laser system tunable to UV, visible, and IR wavelengths (230-1050 nm), providing the necessary flexibility for feasibility studies and testing of a wide range of fluorophores. An inverted microscope equipped with a spectrograph and CCD camera enables imaging of capillary end faces (Figure 1) as well as monitoring the intensity and spectral response of the fluorophore. Initial tests focused on quantifying light throughput dependence on capillary IDs (wall thickness), capillary lengths, capillary coil diameter, and wavelengths. A UV-VIS spectrophotometer was also used to characterize the spectral characteristics and performance as described below.

3 Wolfbeis, Otto S. Trends in Analytical Chemistry (1996), 15(6), 225-232.

4 Messica, A.; Greenstein, A.; Katzir A. Applied Optics (1996), 35(13) 2274-2284.

5 Clonis et al. Biosensors & Bioelectronics. 2002. 17, 61-69

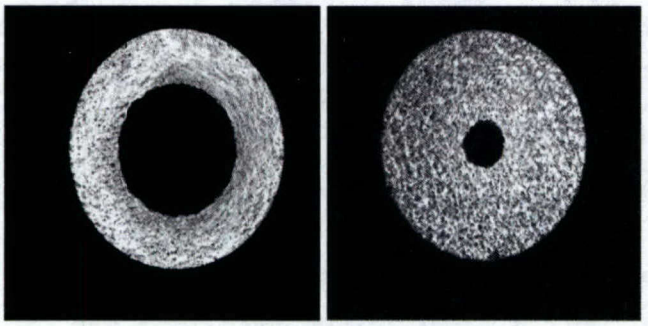

Figure 1. CCD images of end faces for capillaries of 50 μm (left) and 150 μm IDs.

Table 1. Percent light throughput as a function of capillary ID, length, and wavelength.

	Capillary length (λ = 460 nm)			Wavelength (50 μm ID, 1 m in length)		
ID	0.50 m	2.0 m	3.0 m	400 nm	460 nm	545 nm
50 μm	37 (1.2)*	39 (0.7)	41 (0.8)	41 (1.2)	42 (0.7)	43 (4.5)
150 μm	39 (0.9)	39 (0.3)	39 (0.8)	n.d.	n.d.	n.d.

*Values reported as a percentage. Numbers in parentheses are standard deviations for n = 10. n.d.= not determined.

Results of numerous initial studies indicated that about 40% of the incident laser power was transmitted through capillaries of both 50 and 150 μm ID (360 μm OD). This value is mostly controlled by loss of light at the capillary end face. As shown in Table 1, the throughput is consistent regardless of capillary ID or length, or laser wavelength. Throughput is repeatable when capillaries are removed and replaced in the apparatus. With the high throughput, a relatively low power light source (e.g. LED) should provide sufficient intensity for fluorescence sensing. The observed reproducible coupling of source and FOCAP will aid comparison of different FOCAP sensor reagent immobilization schemes.

Fluorescence Characterization

During the initial stages of fluorescence testing, several sources of background signals were discovered and overcome. Besides typical problems such as small light leaks in the optical system, the polyimide coating on the exterior of the capillary has significant background fluorescence. Removal of 0.5 cm of this material at the end face receiving the laser beam eliminates this as a source of background fluorescence, yet still leaves the end of the capillary easy to handle.

Detection of fluorescence from an immobilized fluorophore was also measured. Amine reactive Oregon Green dye was attached to capillary walls modified with aminopropyltriethoxy silane following the scheme shown in Figure 2. An absorbance spectrum of the modified capillary waveguide confirmed that the Oregon Green had been successfully attached. Fluorescence of the immobilized fluorophore was detected on the same capillary. These studies are continuing in order to determine the most reproducible and chemically stable immobilization conditions.

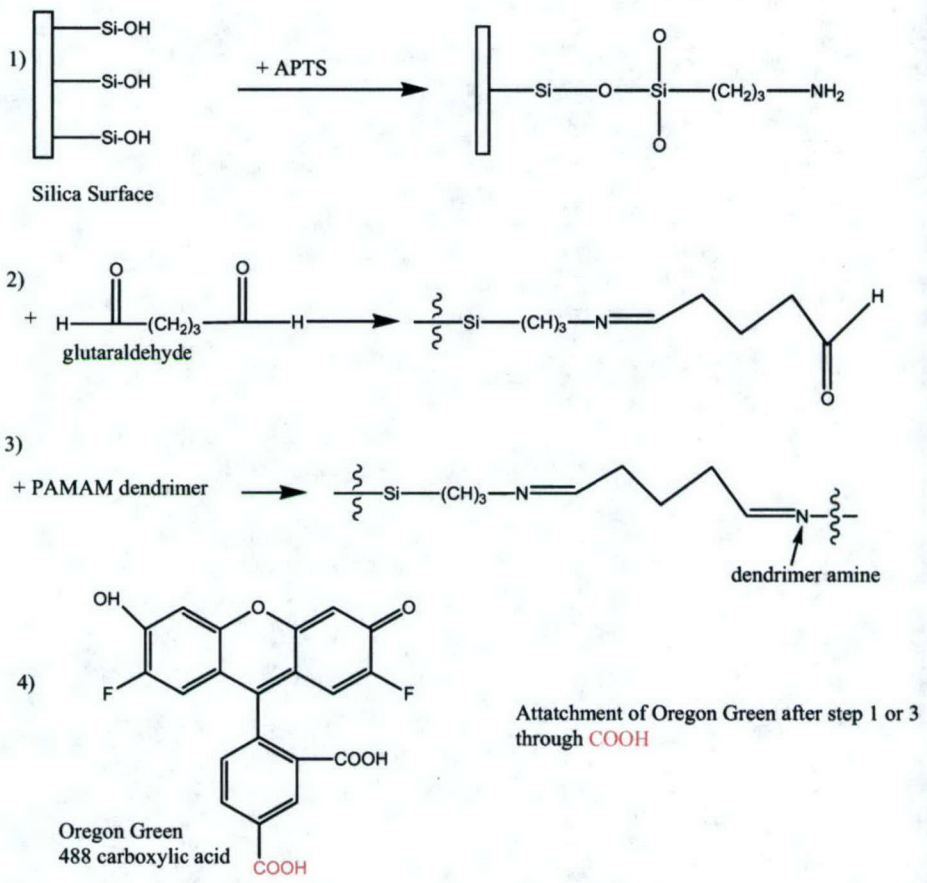

Figure 2: Schematic representation of the capillary surface modification procedures utilized.

Characterization of long pathlength capillary waveguides for evanescent chemical sensing applications

(This section is a summary of a paper published by SPIE[6].)

Light-guiding FOPAC tubing has promising applications in the field of chemical sensors. An evaluation of the light guiding properties of these novel capillaries was performed by coupling the light source from a spectrophotometer into a capillary waveguide. Light propagation in these waveguides occurs within the capillary wall as opposed to liquid core waveguides where light traverses the solution-filled inner core. Figure 2 shows a cross section of the capillary construction and illustrates how light is transmitted down the waveguide. The tubing consists of a synthetic fused silica capillary wall surrounded by a doped silica cladding and a polyimide outer coating. The capillary tubing has inner core diameters (ID) of 50, 150, or

6 B. Keller, M. DeGrandpre, and C. Palmer, SPIE Proceedings, Chemical and Biological Point Sensors for Homeland Defense II 5585, 143-51, (2004).

250 μm with an outer diameter of 360 μm with 0.22 numerical aperture (NA). Light enters the capillary sidewall at point B and experiences total internal reflection at points B and C. The evanescent field penetration from the capillary wall into the capillary core (sensing region) occurs at point C.

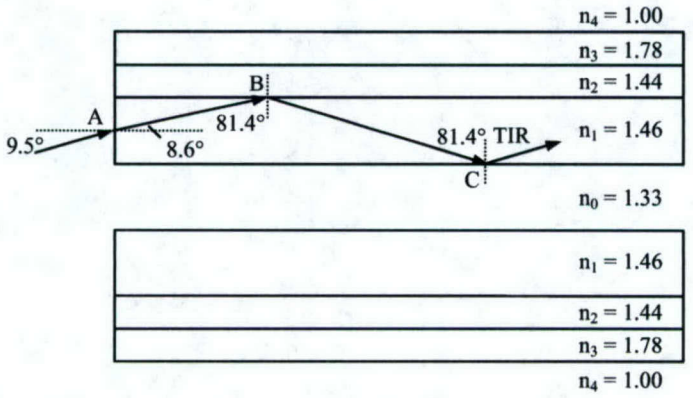

Figure 2. Ray-tracing diagram for light entering the waveguide at the capillary end face. Refractive indices are 1.33 methanol solution capillary core, 1.46 synthetic fused silica capillary wall, 1.44 doped fused silica cladding, 1.78 polyimide coating, and 1.00 air. Light approaches the end face at 9.5° and is refracted into the glass at point A. At point B the ray at 81.4° experiences internal reflection ($\theta_c = 81.2°$), which also occurs at point C ($\theta_c = 65.7°$) and total internal reflection occurs within the capillary wall.

The sensitivity of evanescent absorbance depends upon the depth of penetration of the evanescent field into the absorbing medium and the number of internal reflections that occur within the waveguide. The depth of penetration (d_p, $1/e$ depth) of the evanescent wave is given by Equation 1 where θ is the incident angle normal to the interface and λ is the evanescent field wavelength:[7]

$$d_p = \frac{\lambda}{2\pi (n_1^2 \sin^2 \theta - n_0^2)^{1/2}} . \qquad (1)$$

The depth of penetration of the evanescent wave in a fiber or capillary waveguide is related to the effective pathlength of an evanescent absorbance measurement. The effective pathlength of the capillary was determined by comparing capillary waveguide and conventional absorbance spectrophotometry measurements. The effective pathlength ratio (EPLR) in Equation 2 includes the absorbance measurements from evanescent and cuvette cells (A_{evan} and A_{spec}, respectively) along with the capillary length and cuvette pathlength (b_{cap} and b_{spec}): [8]

$$EPLR = \left[\frac{A_{evan}}{A_{spec}}\right]\left[\frac{b_{spec}}{b_{cap}}\right] . \qquad (2)$$

7 B. Culshaw and J. Dakin, Optical Fiber Sensors Vol. 3: Components and Subsystems (Artech House, Inc. 1996).

8 M. Belz, P. Dress, A. Sukhitskiy, and S. Liu, Proc. SPIE 3856, Internal Standardization and Calibration Architectures for Chemical Sensors (Boston), 271-281, (1999).

In this study a series of thiacyanine dyes (Table 2) with distinct peak absorbances across the visible spectrum allowed wavelength dependent characterization of the optical properties of these fused silica capillary waveguides. The depth of penetration of the evanescent wave and the dependence of the evanescent absorbance on capillary dimensions (length and wall thickness) and dye concentration were determined.

Table 2. Laser grade thiacyanine dyes with molecular weight, peak visible absorbance wavelength, and molar absorptivity.

Abbreviation	Molecular weight (g/mol)	λ_{max} (nm)	ε_{max} (L/mol cm)
DTC	466.40	424	8.30×10^4
DTCC	492.44	557	1.62×10^5
DTDC	518.48	657	2.47×10^5
DTTC	544.52	758	1.95×10^5

Experimental

FOCAP absorbance measurements were performed with an Agilent 8453 UV-visible spectrophotometer equipped with a fiber optic coupler kit (Custom Sensors and Technology, Inc.) as illustrated in Figure 3.

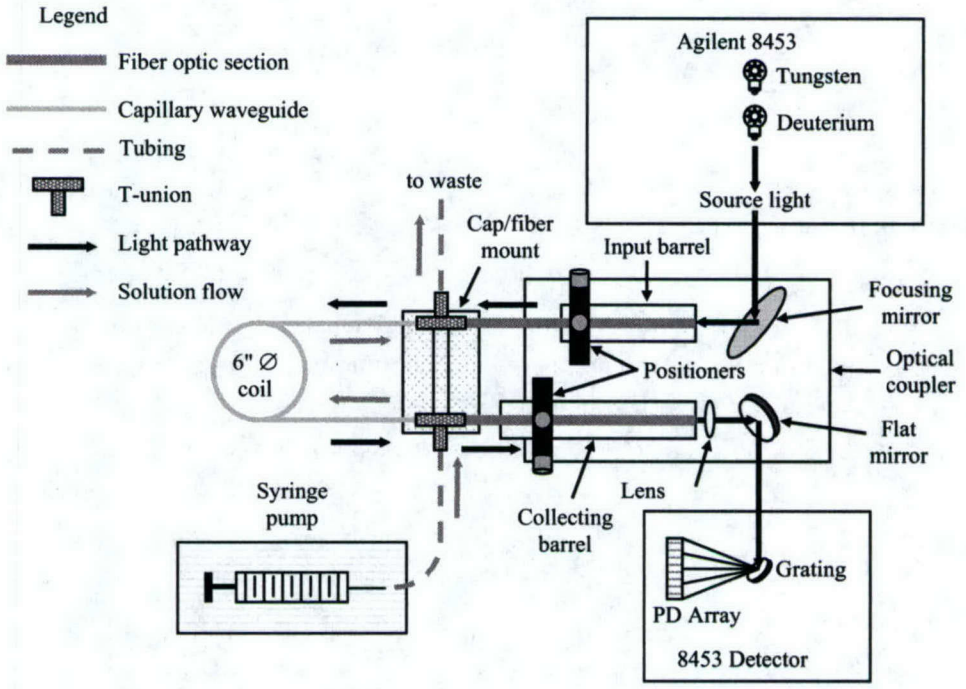

Figure 3. Capillary evanescent wave absorbance experimental apparatus using Agilent 8453 spectrophotometer and Custom Sensors, Inc., fiber optic coupler.

Results

The evanescent absorbance dependence upon solution concentration is nonlinear for each dye absorber in Figure 4. This dependence has been observed in fiber optic evanescent sensors

and was attributed to adsorption of ionic dye onto a fused silica surface.[9]

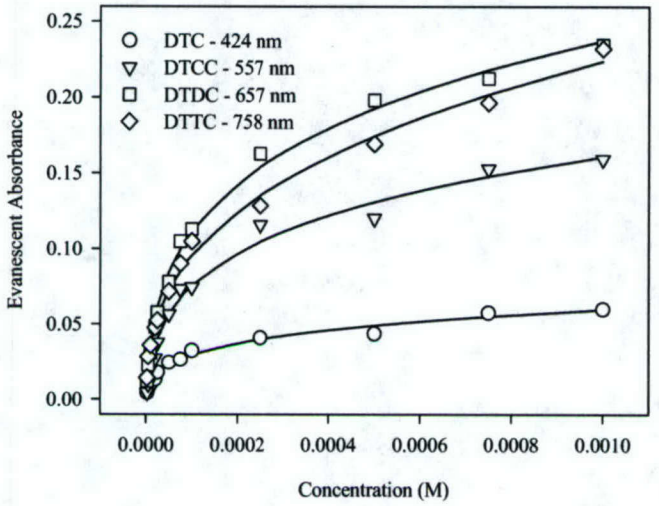

Figure 4. Evanescent absorbance values of thiacyanine dyes in a 4 m 150 μm ID capillary showing nonlinearity with concentration.

Figure 5 shows the effective pathlength ratio calculated from Equation 2 using the solution absorbance in a cuvette (0.1 mm) and the evanescent absorbance values in Figure 5. The evanescent sensing region is on the order of 10^{-5} to 10^{-6} meter per meter of capillary. The EPLR is also shorter at the shorter wavelength measurements as predicted by Equation 1.

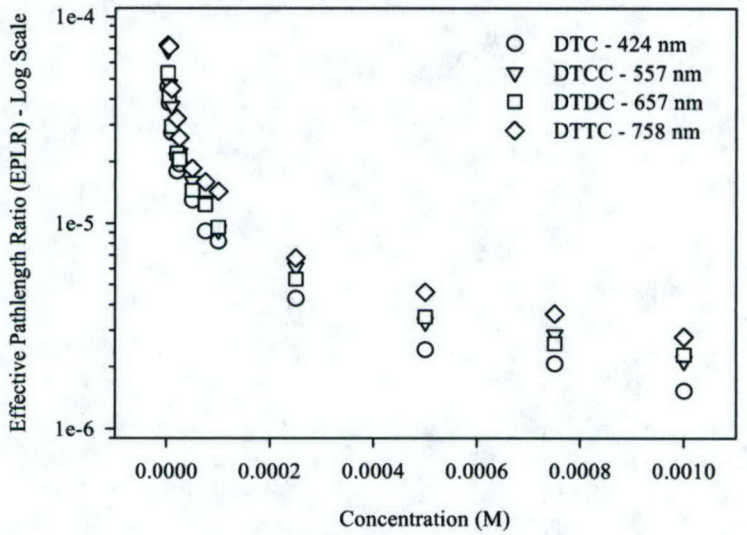

Figure 5. Log scale plot of effective pathlength ratios (EPLR) of thiacyanine dyes determined from conventional absorbance measurements in a 0.1mm cuvette and the evanescent absorbance values in Figure 4.

9 V. Ruddy, B. D. MacCraith, and J. A. Murphy, J. Appl. Phys. 67(10), 6070-4, (1990). B. D. Gupta and S. K. Khijwania, Fiber and Intergrated Optics 17, 63-73, (1998).

The wavelength dependence of the EPLR is explained by the deeper evanescent field penetration at longer wavelengths (Equation 1). The ratio of the depth of penetration (d_p ratio) at each absorbance peak wavelength was determined from the ratio of the EPLR values of DTC, DTCC, and DTDC relative to DTTC as shown in Table 3. Theoretical values were determined from Equation 1 assuming the same distribution of launch angles θ for each wavelength.

Table 3. Experimental and theoretical wavelength dependent evanescent depth of penetration ratios of thiacyanine dyes.

Dye (λ)	Experimental d_p ratio	Theoretical d_p ratio
DTC (424 nm)	0.60 ± 0.07	0.56
DTCC (557 nm)	0.78 ± 0.10	0.73
DTDC (657 nm)	0.73 ± 0.07	0.86
DTTC (758 nm)	1.00 (normalized)	1.00 (normalized)

The effects of increasing capillary length upon the evanescent absorbance values were also investigated. Figure 6 shows the evanescent absorbance of DTDC-filled capillaries up to 20 m in length. Evanescent absorbance is fairly linear in capillaries up to 10 m but begins to level off quickly with increasing capillary length.

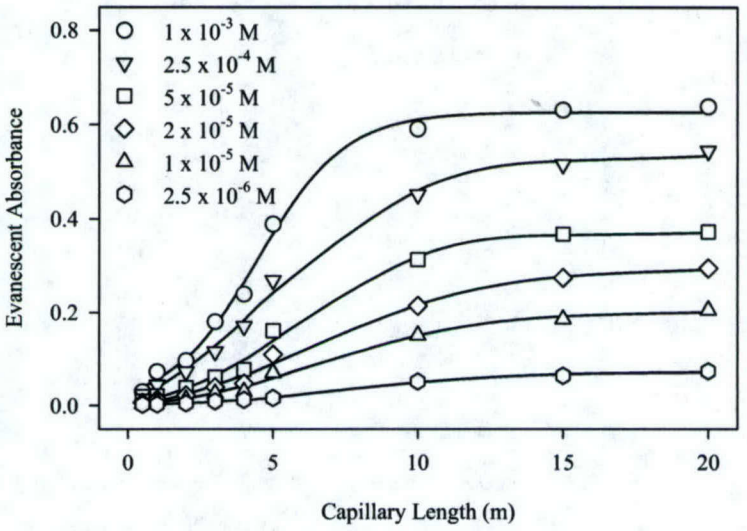

Figure 6. Evanescent absorbance values for DTDC solutions at 657 nm measured with increasing capillary length (all 150 μm ID).

The sensitivity of evanescent absorbance with various capillary inner diameters (ID) was tested. The thickness of the capillary wall determines the number of reflections that light rays will experience. More reflections off the capillary inner wall increase the evanescent sensing volume. Thinner-walled capillaries have a higher number of internal reflections per meter than

thicker-wall capillaries. Figure 7 shows the evanescent absorbance values at different concentrations of DTDC for 5 m capillaries with inner hollow core diameters of 50, 150, and 250 μm each with the same outer diameter (360 μm). Capillaries of 50, 150, and 250 μm ID have calculated inner reflection ratios of 1, 1.7, and 6.9 respectively. Experimental ratios determined from Figure 5 are 1, 2.0 ± 0.9, and 6.5 ± 1.2.

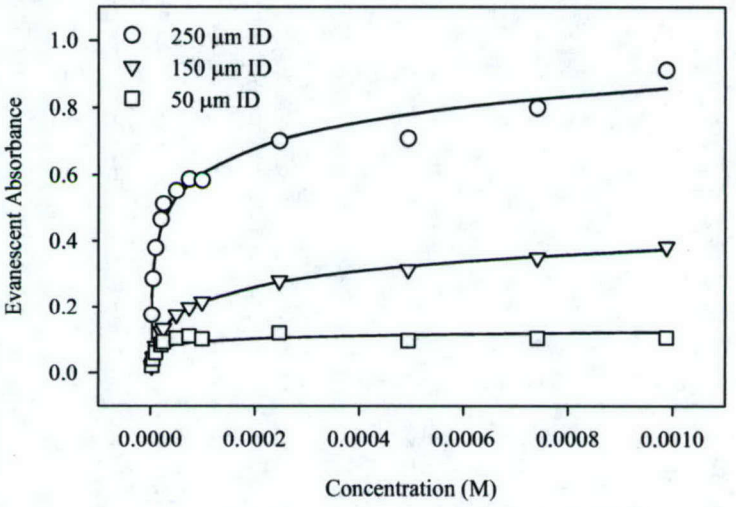

Figure 7. The sensitivity of capillaries with different wall thickness was tested by measuring evanescent absorbance of DTDC solutions in capillaries of 50, 150, and 250 μm ID. Capillaries with larger inner diameter or decreasing wall thickness have greater absorbance sensitivity than capillaries with thicker walls due to the greater number of reflections in the thin-walled capillaries.

Conclusions

Study of the evanescent light-guiding properties of these waveguides is warranted to aid in the development of new sensing devices. Absorbance due to the evanescent effect showed a linear dependence upon capillary length to 10 m as predicted by theory but showed an unexpected plateau with longer FOCAPs. Evanescent absorbance was non-linear with increasing dye solution concentration. The likely cause of this dependence may be surface adsorption of the ionic dye to the fused silica capillary wall. The effective pathlength of these capillaries is small and limits sensitivity of shorter capillaries but the sensitivity is increased in thin-wall capillaries because of the increased number of reflections per meter.

Development and characterization of chemistries for immobilization of selective reagents

The enzyme acetylcholinesterase (AChE), immobilized on fiber optics, FOCAP sensors, or electrodes can be utilized for the selective and sensitive detection of nerve agents. We have investigated chemistries for the immobilization of AChE on FOCAP sensors and on silica surfaces of similar chemistry.

Enzyme Immobilization

Both silica particles and fused silica capillary surfaces have been modified with acetylcholinesterase using a 3-step scheme that involves reaction of the surface with aminopropyl triethoxy silane (APTS), glutaraldehyde, and AChE.[10] Silica particles and capillary have also been modified using a 5-step scheme developed during the course of this project that involves reaction of the surface with APTS, glutaraldehyde, generation 4 PAMAM dendrimer, glutaraldehyde, and AChE. The purpose of modification with the dendrimer in the 5-step sequence is to increase the loading of AChE on the surface.

Silica particles were purchased from Macherey-Nagel (Nucleosil 1000-10). The silica particles were added to a round bottom flask and immersed in deionized water (DI). To that solution was added 3-aminopropyltrimethoxy silane and the mixture was heated to 80°C and let react for 90min. Then glutaraldehyde was added to the solution and let react for 20 min. Next, generation 4 poly(amido amine) (PAMAM) dendrimer was added to the round bottom and let react for 90min. After this glutaraldehyde was added to the round bottom again for 20 min. Finally Eel or recominbinant mouse AChE was added to the round bottom and let react for 90 min. The modified silica particles were tested for enzyme activity using Ellman's reagent.

Elemental analysis of the modified silica particles shows an increase in carbon and nitrogen content with each step in the sequence (Table 4), although less than monolayer coverage is observed and increases with immobilization of AChE are not as great as expected.

Table 4: Elemental Analysis of Modified Silicas

Synthetic Step	% Carbon by wt.	% Nitrogen by wt.
1. APTS	0.67 +/- 0.02	0.22 +/- 0.02
2. Glutaraldehyde	1.17 +/1 0.02	0.18 +/- 0.02
3. Generation 4 PAMAM	2.24 +/- 0.02	0.67 +/- 0.02
4. Glutaraldehyde	2.92 +/- 0.02	0.63 +/- 0.02
5. Eel AChE	3.16 +/- 0.02	0.73 +/- 0.02

10 Singh, A. K.; Flounders, A. W.; Volponi, J. V.; Ashley, C. S.; Wally, K.; Schoeniger, J. S. Biosensors & Bioelectronics 1999, 14(8-9), 703-713.

It is not possible to conduct elemental analysis on modified capillaries because of the polymer coating. Instead, measurements of electroosmotic flow were used to indicate that the surface been modified with APTS after step 1 and further modified with dendrimer after step 3. Cathodic flow was greatly reduced on modification with APTS, and a strong anodic flow was observed after modification with dendrimer. The anodic flow clearly indicates a positively charged surface with a large number of amino groups after dendrimer immobilization.

AChE-modified surfaces showed measurable AChE activity (Ellman Assay), both on silica particles and on capillary walls. When the silica was rinsed with water, the rinsate did not show measurable AChE activity. Although the modified surfaces did show measurable activity, it was not possible to quantify the activity sufficiently to permit comparison of modification schemes. A separate assay of acetylcholinesterase activity, known as the amplex red assay, confirmed that the immobilized enzyme was active. However, this method also failed to permit quantitative determination of enzyme kinetics.

Several chemical schemes were evaluated for the determination of total immobilized protein. The glutaraldehyde-modified silicas have a pink color that interferes with most UV-Vis spectroscopic assays. For example, the commonly used BCA assay was found to be incompatible with the immobilization chemistry as the method gave a large signal for glutaraldehyde-modified surfaces even in the absence of immobilized protein. It was discovered during the course of this project that reported methods for the determination of enzyme activity and total protein are not directly amenable to the characterization of immobilized enzymes. We have thus embarked on a project to develop reliable methods for these determinations such that various modification chemistries used for sensor development can be evaluated.

Final Report Year 1

Portable Chemical Agent Detection System:
Differential Reflectometer and Light Scattering Approaches
Paul H. Holloway, Rolf Hummel and Mark Davidson
Department of Materials Science and Engineering and MICROFABRITECH
University of Florida
Gainesville, FL 32611-6400

Summary

- Films of TNT deposited onto Si wafers with a SiO_2 surface layer showed differential reflectance peaks at 250, 460 and 760 nm.
- FTIR data show a fingerprints structure for TNT.
- Crystalline TNT scattered 707 nm light more strongly than other materials.

Objectives

The objectives of this research are to demonstrate the effectiveness of the differential reflectometer and optical scattering for sensitive, accurate detection of explosives like TNT.

Approach

The current differential reflectometer with wavelength capabilities from 300 to 800 nm will be used to identify reflectance peaks in the near UV, visible and near IR wavelength regions to detect the molecular absorption signature of vapors from explosive materials. In addition, the scattering of light from crystalline explosive materials will be studied.

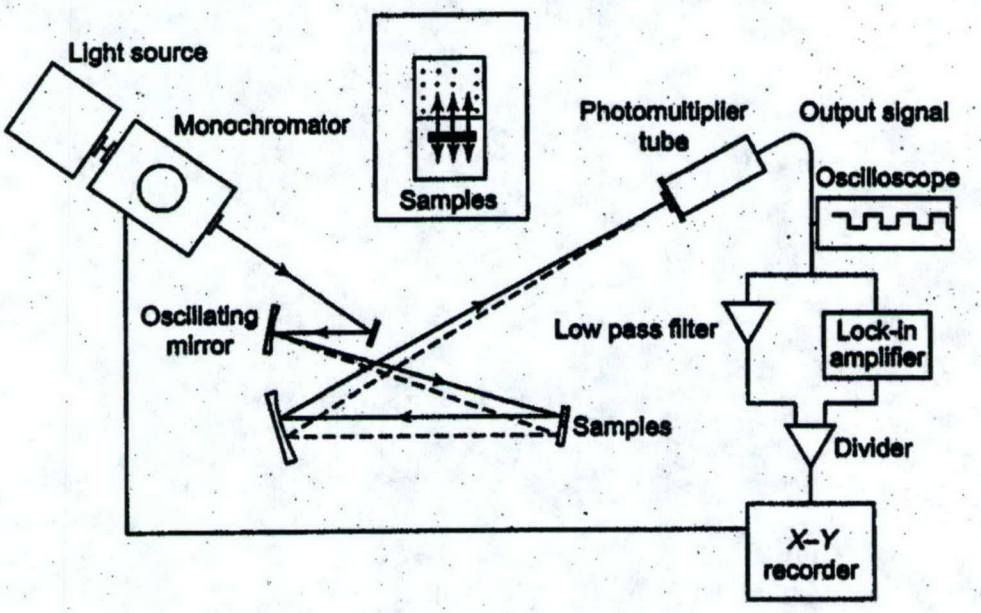

Figure 1. Schematic of existing differential reflectometer.

Part I: Differential Reflectometer Detection of TNT

The existing differential reflectometer is schematically shown in Figure 1. The light source and monochromator are capable of scanning over a wavelength of 200 to 800 nm. Samples of 98% pure TNT were purchased from Chemiservices, dispersed in acetonitrile solvent at concentrations of 36-144 mg/ml, and deposited onto oxidized Si wafers by applying a droplet, with or without spin-coating, and allowing the acetonitrile solvent to evaporate, leaving a 'film' of TNT. A typical optical micrograph of such a film is shown in Figure 2, showing regions of crystallized TNT. The differential reflectance spectra taken from such an area are shown in Figure 3.

Figure 2. Optical micrograph of layer of TNT on a thin film on Si wafer.

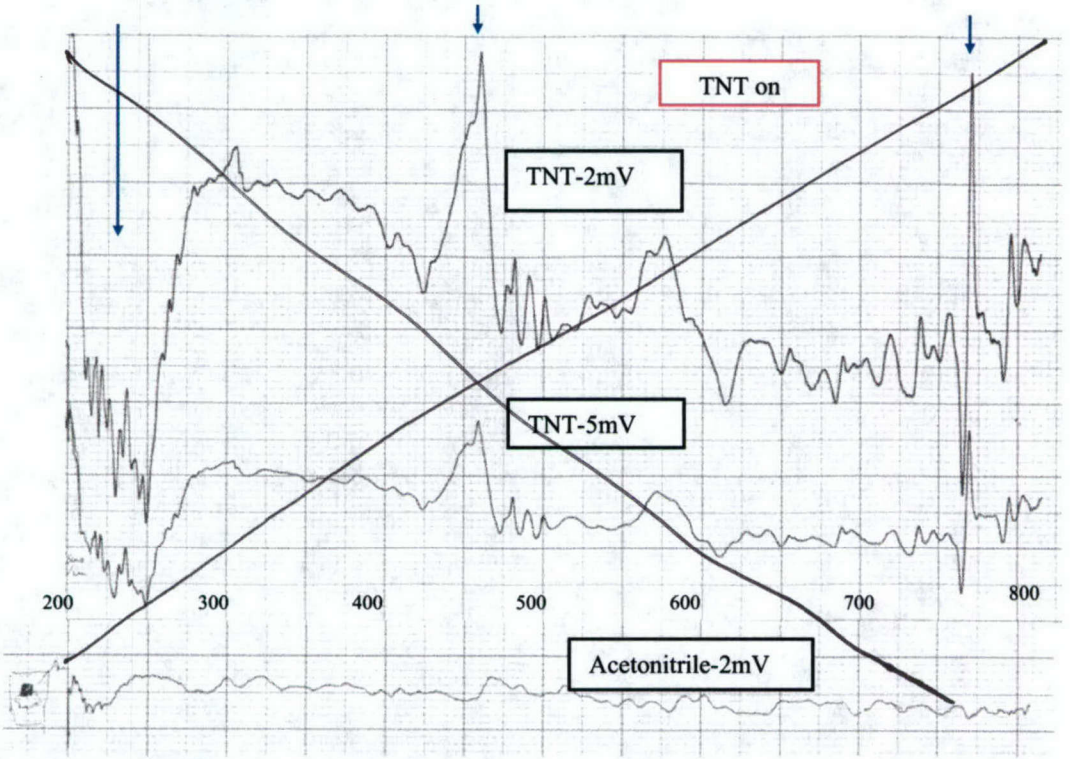

Figure 3. Differential reflect spectra from different areas of TNT film on a Si wafer with an unknown thin film coating. The spectra were recorded at different sensitivity to show repeatability of the peaks. Note the absence of peaks from the solvent.

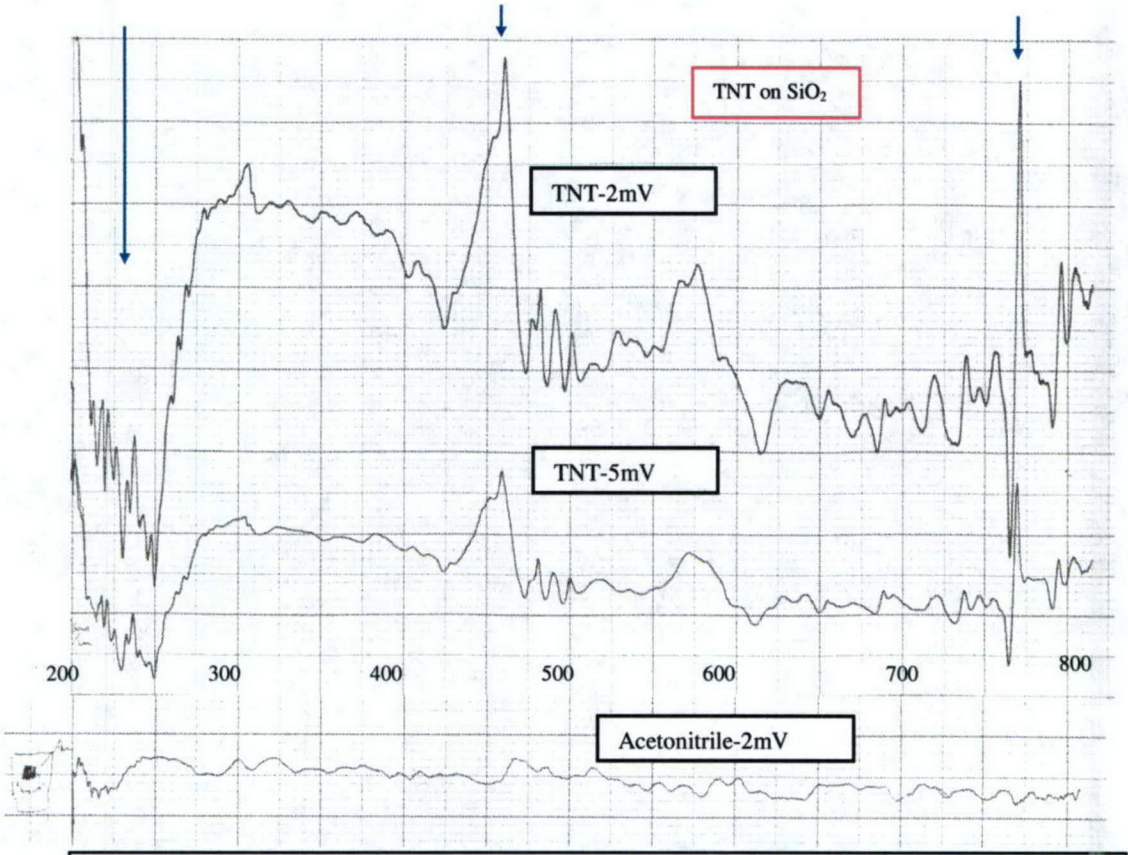

Figure 3 Differential reflect spectra from different areas of TNT film on a Si wafer with an unknown thin film coating. The spectra were recorded at different sensitivity to show repeatability of the peaks. Note the absence of peaks from the solvent.

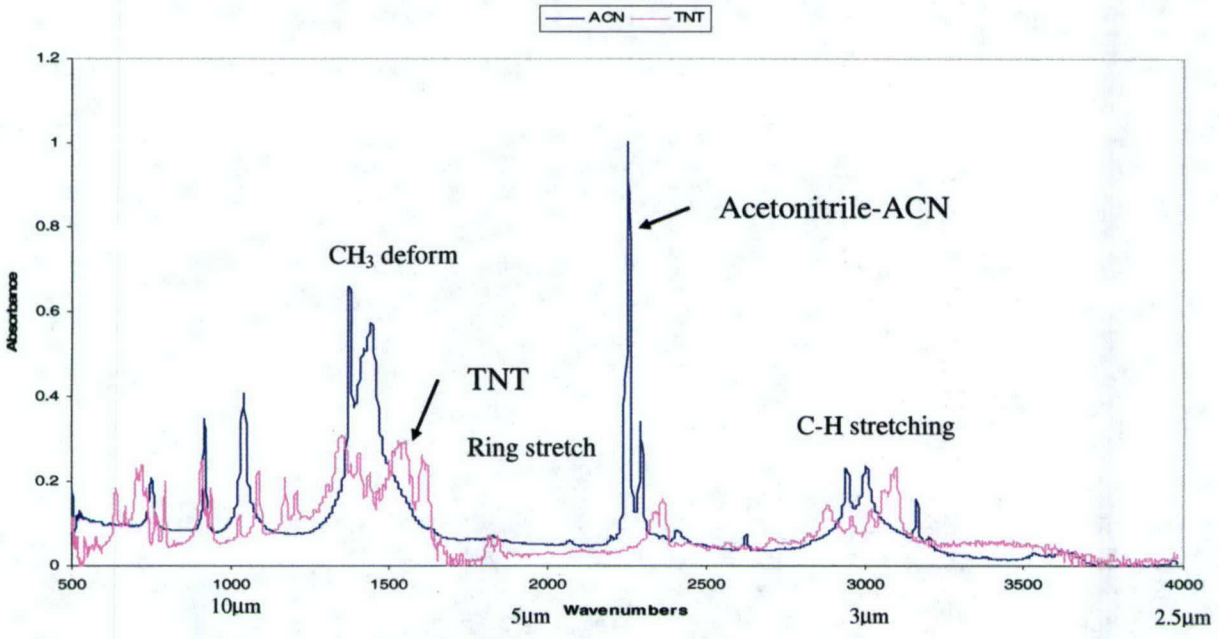

Figure 4 FTIR spectra from a TNT film and from the acetonitrile solvent.

These spectra show peaks in the ΔR/R data at wavelengths of 220-250 nm, 460 nm and 760 nm. These peaks are symptomatic of the TNT layer, and their origins in the visible to near infrared regions are though to result from a TNT-OH transient species reported in the literature. Peaks in the 250 nm range are thought to result from UV absorption by the TNT molecule, as also reported in the literature. When similar TNT films were dispersed on a Si wafer metallized with Au, only the 250 nm peak was observed.

Finally, the FTIR spectrum from a TNT film and the acetonitrile solvent were recorded as shown in Figure 4. It is clear that the fingerprint of TNT is different from that of the solvent. The range of the FTIR spectra does not overlap that of the DR therefore the peaks shown in Figure 3 do not appear in Figure 4. Preliminary FTIR data over an extended range down to a wavelength of 700 nm show some structure between 700 and 800 nm which could be similar to the DR peak at 760 nm, but further study is required to verify this fact.

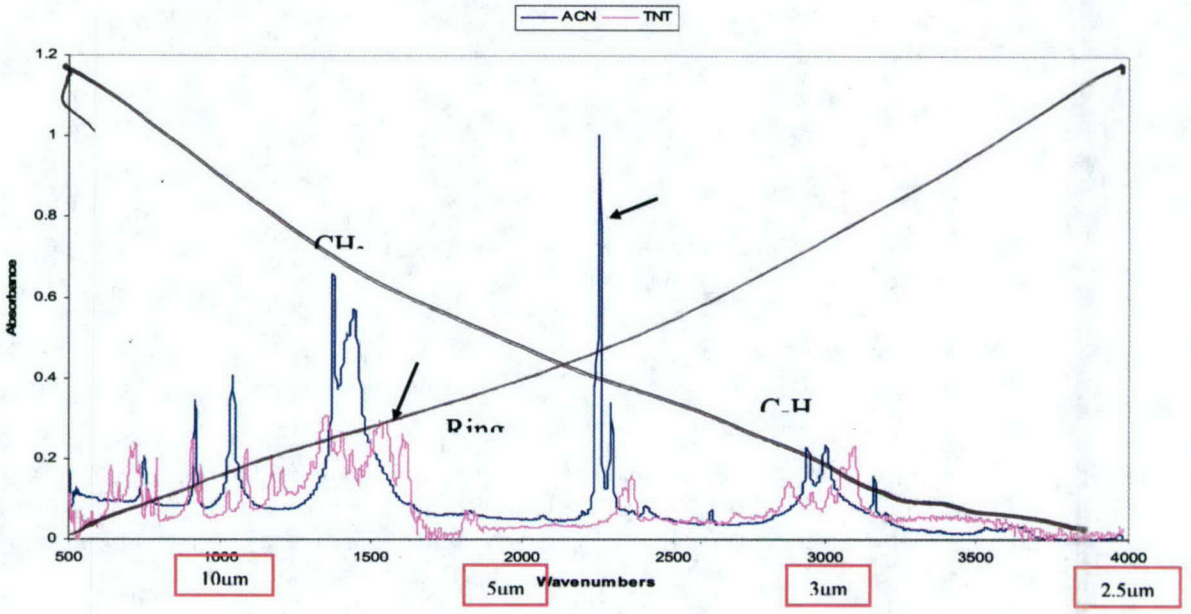

Figure 4. FTIR spectra from a TNT film and from the acetonitrile solvent.

Part II: Detection of TNT by Laser Excitation

Initially we mistakenly believed that TNT, when exposed to an appropriate exciting light source, had a characteristic emission spectrum (sharp photoluminescence peak) at ~707 nm with minor peaks at 666 and 728 nm (see Figure 5). However, we subsequently have discovered that the

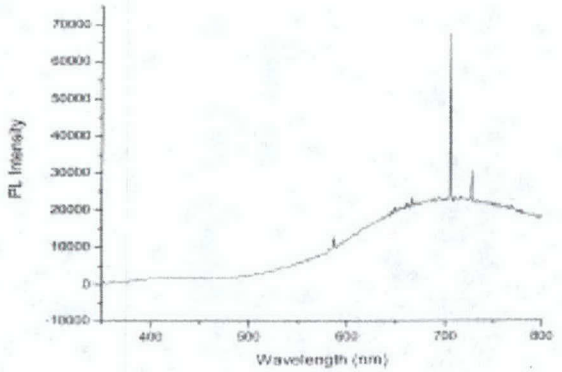

Figure 5. Photoluminescent spectrum from TNT excited by HeCd laser irradiation at 325 nm.

interference filter used to 'remove' the plasma lines (impurity emission lines from the HeCd laser) was defective. Specifically, the interference filter has a low optical density and allowed light with wavelengths between ~650-750 nm to scatter from the sample. The HeI line at 707 nm passed with the least attenuation and therefore was detected when scattered by the TNT (and other explosives) dispersed on various substrates. The minor peaks at 666 and 728 nm are also HeI lines from the laser plasma, but attenuated to a larger extent by the interference filter. While these peaks at 666, 707 and 728 nm do not result from a unique emission from TNT, they are detected much more strongly when crystalline TNT is present to scatter the HeI radiation at these wavelengths. This is apparently true for other explosive materials as well.

To verify that the scattered HeI signal at ~707 nm was more intense from TNT, we have recorded the scattered spectra from a number of materials as shown Figure 6. Spectra from two different types of perfume, toluene, lighter fluid (naptha), benzene and naphthalene are shown. It is obvious that none of these materials scatter the HeI line at ~707 nm in a manner similar to crystalline TNT. However it is unclear whether this scattered intensity could be used to detect explosive material like TNT.

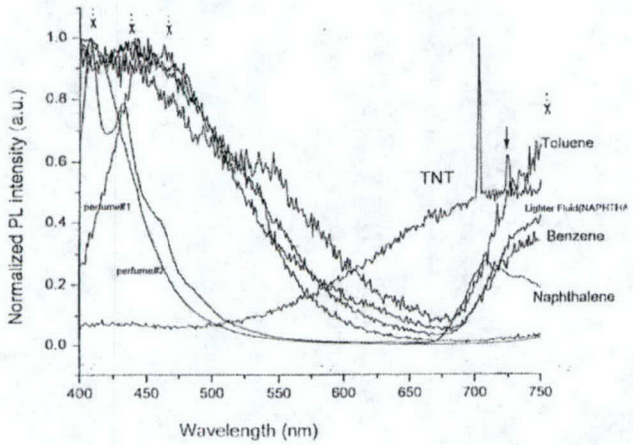

Figure 6. Scattered light spectra from possible interferents for TNT.

Publications

None ("Detection of Explosive Materials by Photoluminescence" by Rolf E. Hummel, A. Fuller, K. Kim and Paul H. Holloway was submitted, reviewed and accepted by Applied Optics, but withdrawn before publication upon discovery of the bad interference filter.)

Presentations

Portable Chemical Detector Kickoff Meeting, University of Montana, Missoula, MT, July 24, 2003.

Patents

None ("System and Method for Detection of Explosive and Other Target Materials", Kwanghoon Kim, Rolf E. Hummel, Paul H. Holloway, and Anna Fuller; application submitted January 22, 2004, was withdrawn January, 2005).

Post Doctoral Associates and Graduate Students

Dr. Nigel Shepherd, Post Doc
Kwanghoon Kim, GRA
Anna Fuller, GRA

Final Report Year 1
For the period: March, 2003 – September, 2004
An Ultra-sensitive Approach for the Detection of Explosive Vapors
Submitted by
J. D. Winefordner, Nicolo Omenetto and B. W. Smith
Department of Chemistry
University of Florida
Gainesville, FL 32611

Introduction and Background

Sensitive, portable methods for the rapid chemical characterization of vapors, liquids, solids and individual particles are important to a wide range of fields. The focus of this research program is the development of a portable instrument for the ultra-sensitive detection of explosive vapors and particulates, an especially important problem in counter-terrorism, landmine detection[11] and pollution control. A recent review[12] points out that "Overall, detector dogs still represent the fastest, most versatile, reliable real-time explosive detection device available." Clearly, there is a pressing need for improved instrumental techniques for this problem.

Steinfeld and Wormhoudt[13] have succinctly reviewed the field of explosives detection. They emphasize the critical aspects of the problem which include the low vapor pressures common to most explosive materials, the limited sample sizes typically available for analysis and the problem of interferences. In addition, explosives are often deliberately concealed which further frustrates reliable detection. Detection strategies can focus on solid or vapor phase sampling, depending on the physical situation. A very wide range of analytical techniques have been evaluated for explosives detection. Without reviewing them in detail here, one can generally conclude that further increases in sensitivity are still needed, especially for vapor phase detection, which is the most promising approach for *in-situ* detection of explosives on humans, luggage, vehicles and shipping containers and for the detection of buried landmines. For really useful detection in these environments, we seek a method which is capable of detecting explosive vapors at low to sub-parts per trillion levels.

All of the common chemical explosives and related constituents (for example, TNT, NG, EGDN, RDX, PETN, TATB, AN and UN) contain nitrogen oxide functional groups and thus are amenable to detection by sensing of NO_x species. These may be released by a photofragmentation process involving the release of a weakly bound NO_2 functional group in the ground electronic state after absorption of light at 226 nm. The NO_2 molecule then absorbs another photon, is excited to the $2\ ^2B_2$ electronic state and undergoes rapid predissociation to

---

[11] T. F. Jenkins, D. C. Leggett, P. H. Miyares, M. E. Walsh, T. A. Ranney, J. H. Cragin and V. George, Chemical signatures of TNT-filled land mines, *Talanta*, **54**, 501-513 (2001).

[12] K. G. Furton and L. J. Myers, "The scientific foundation and efficacy of the use of canines as chemical detectors for explosives," *Talanta*, **54**, 487-500 (2001).

[13] J. I. Steinfeld and J. Wormhoudt, "Explosives Detection: A challenge for physical chemistry," *Annu. Rev. Phys. Chem.*, **49**, 203-232 (1998).

produce NO in the ground vibrational state of the ground electronic state. Both NO and NO_2 can be detected with extremely good detection limits by chemiluminescence. The goal of this proposal is to detect a very small change in the local concentration of nitrogen oxides (derived from explosive vapors). The challenge is to develop a measurement system which is highly sensitive to nitro-groups and can detect a small change in their concentration against an ambient background level of up to some tens of ppb. The approach which we propose is to create NO or NO_2 via efficient photofragmentation of explosive vapors with subsequent detection using the most sensitive available technique, luminol or ozone chemiluminescence. Technical barriers which need to be addressed include a means by which to remove ambient NO and NO_2 prior to the photofragmentation (thereby greatly reducing the background signal), optimization of the photofragmentation spectroscopy for maximum yield of NO or NO_2 from the explosive vapor and the design and optimization of a highly sensitive ozone or luminol-chemiluminescence detection system. Finally, all aspects of the instrument need to be considered in the context of ultimate portability.

Overview of Research Plan

The technical barriers mentioned above will be studied in parallel experiments using TNT, PETN and RDX as model compounds. These three explosives have 300 K equilibrium vapor pressures of 13, 0.026 and 0.0084 ppbv, respectively, thereby covering a wide range of concentrations[14]. The concentrations of all three can be dramatically, and safely, increased with temperature up to 400 K, yielding equilibrium concentrations of about 10^5x higher. Global vapor pressure expressions for many explosive compounds have been published by Dionne, *et al.*[15].

The main objective during the first two years will be the study of the photofragmentation characteristics of these model explosive vapors with the goal of optimizing the creation of either NO or NO_2 and the evaluation of the chemiluminescence which produce in reaction with ozone or which they induce in luminol. These studies will be done using a 193 nm excimer laser and conventional xenon flashlamps in temperature-controlled flowing or quiescent sample cells at varying vapor concentrations. Simultaneously we will determine the most effective means by which to remove ambient background nitrogen oxides prior to photofragmentation of the explosive vapor. This must be done without removing the analyte explosive vapor. Possibilities include selective adsorption, chemical reaction or an additional photolysis scheme. The critical issue with any adsorptive or reactive NO_x removal mechanism is that it not remove the analyte vapor as well. This may prove difficult to achieve because explosive vapors are known to be easily lost to wall adsorption during transport.

An alternative to adsorption removal is to incorporate an additional broadband photolysis scheme which takes advantage of the selectivity of the luminol-CL detection for NO_2. NO_2 is very efficiently photodissociated by photons of wavelength < 420 nm[16] and could then be

---

[14] B. C. Dionne, D. P. Rounbehler, E. K. Hobbs, Jr. and D. H. Fine, "Vapor pressures of explosives," *J. Energetic Mater.*, 4, 447-472 (1986). P. A. Pella, "Measurement of vapor pressures of TNT, 2,4-DNT, 2,6-DNT, and EGDN," *J. Chem. Thermodynam.*, **9**, 301-305 (1977).

[15] B. C. Dionne, D. P. Rounbehler, E. K. Hobbs, Jr. and D. H. Fine, "Vapor pressures of explosives," *J. Energetic Mater.*, 4, 447-472 (1986).

[16] T. B. Ryerson, E. J. Williams and F. C. Fehsenfeld, "An efficient photolysis system for fast-response NO_2 measurements," *J. Geophys. Res.*, **105**, 26447-26461 (2000).

removed from the sample cell with a few seconds of cw UV illumination (a compact xenon arc lamp is typically used) prior to the laser photofragmentation of the explosive vapors to produce fresh NO_2 for the luminol-CL detection. Optimization of this process would involve studying the intensity and wavelength dependence of both processes to obtain the most efficient dissociation of ambient NO_2 without decomposition of the analyte vapor.

Finally, we have been designing and optimizing highly efficient ozone and luminol-CL detectors. The luminol-NO_2 chemiluminescence spectrum peaks at about 415 nm with about 100 nm FWHM. Limits of detection as low as 10 pptv have been reported[17]. The ozone-NO_2 chemiluminescence spectrum peaks in the spectral range 800-1200 nm with typical limits of detection ranging from 50 pptv to low ppbv. We have also continued the development of a novel inlet system for the collection of particulate samples. Our prototype uses five variable apertures for aerodynamic lenses allowing real time control of the particle size to be interrogated by the laser. Laser excited fluorescence of individual particles will be used as the detection method, ultimately with a frequency doubled power-chip solid state laser. This same laser will also be studied as a source for photofragmentation for vapors. Since laser fluence is important here, the high repetition rate of these lasers (up to 10 kHz) makes them excellent candidates for this application. Regardless of the type of sample detected (vapor or solid), we need to carefully address the issue of real time detection at ambient pressures.

First Year Progress

The first work done this year was an investigation of recent chemiluminescent detection schemes. Chemiluminescence is particularly suited to our investigation due to its well known very low limits of detection. This is due in part to simplicity of the detector setup. Most notable is the lack of an external light source, which in turn eliminates any noise from fluctuations of excitation source, light scattering or external light contamination. At the detection limit, the measurement is detector noise limited. Our detection method is based on the detection of nitrogen oxides produced by photofragmentation of explosive vapors. There are two chemiluminescent reactions which have been widely used for NO and NO_2 detection. Luminol reacts with NO_2 producing light at 425 nm and ozone reacts with NO producing light between 800 and 1200 nm. The basic chemiluminescent reaction is M+O _> MO*_> MO + hv, where M is the luminescing specie, O the oxidizer and MO* the excited state of the fluorophor prior to photon emission. In the luminol reaction the oxidizer NO_2, reacts with luminol creating activated 3-aminophthalate which decays to the ground state with the release of a photon at 425 nm. In the reaction of NO with ozone, the ozone serves as the oxidizing agent and it is excited NO_2 which provides the luminescence with a maximum at about 1100 nm. The prime difference between the two reaction schemes is that the ozone reaction takes place entirely in the gas phase while the luminol reaction takes place at a liquid-gas interface. The typical limits of detection of each method fall within that required for the levels that we wish to detect, 30 ppt for the luminol detector and 10 ppt for the ozone method.

After a review of the two techniques, we decided to simultaneously develop both ozone and luminal approaches for detection. They each have important merits which deserve further research attention. A description of the proposed chemiluminescence detection cell follows.

---

[17] G. J. Wendel, D. H. Stedman, C. A. Cantrell and L. Damrauer, "Luminol based nitrogen dioxide detector," *Anal. Chem.*, **55**, 937-940 (1983).

Chemiluminescent cell design

There are several essential requirements for a sensitive chemiluminescence cell (Figure 1); good reagent/analyte mixing for maximum photon yield, a light tight enclosure to eliminate background radiation and an optical design which is highly efficient. The classical gas phase chemiluminescence cell is composed of a glass sphere with ozone and analyte inlets, and outlets with a reflector on one side and a photomultiplier tube on the other. We have designed a more efficient reaction/detection cell which is light tight and serves as the light-collecting optical element. The parabolic reflector will be machined from a solid block of nickel which will then be gold plated and polished. The gold plating will reduce oxidation by ozone and has good reflectance at the emission wavelength of the ozone reaction. The design of the reaction cell allows it to be directly attached to the cooled pmt housing. In our design, the concentric inlets will increase photon collection due to better mixing of analyte and ozone and creation of the initial emission at the focus of the parabolic mirror.

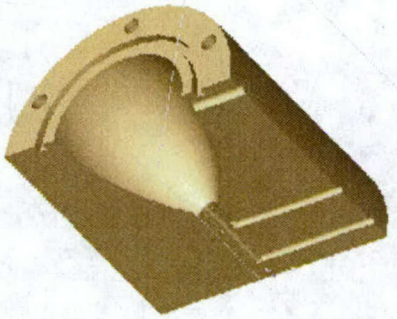

Figure 1: Cutaway of Chemiluminescence cell

For the luminol scheme, we have designed a chamber which bolts directly to the face of a cooled PMT. The luminol is injected with a nebulizer to provide intimate mixing with the gas stream containing NO_2.

Ozone generator

The ozone scheme requires a continuous excess concentration of ozone. It will be designed to use ambient air rather than a pure oxygen source. There are two common ways to create large amounts of ozone, the first being a photodissociation of O_2 followed by a recombination to O_3 , the second using a high voltage to ionize O_2 which combines to form O_3. For our purposes we have initially chosen to use the high voltage

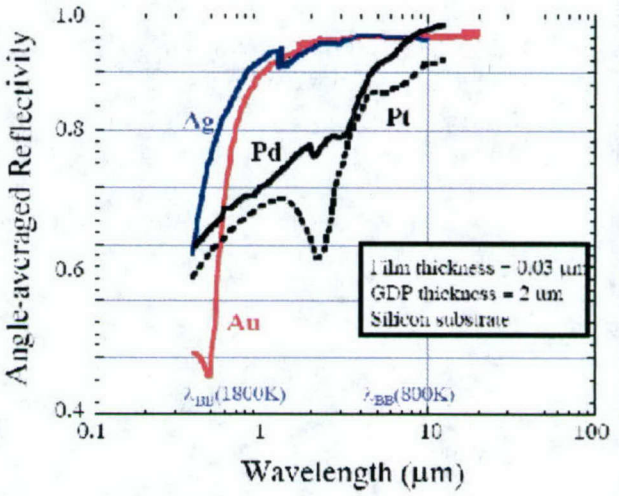

Figure 2: Reflectivity of noble metals
http://www ferp.ucsd.edu/ARIES/MEETINGS/0103/Mau2.pdf

ionization approach. The generator design is similar to commercially available units, except that the cathode and anode plates have been rolled making a cylindrical device as opposed to two plates. This offers three advantages. It allows for better insertion into the inlet system (tubing is connected directly to the inlet and outlet of the generator), the cathode and anode can be more easily cooled increasing ozone production and the outer electrode can be held at ground to reduce risk of electric shock. A prototype ozone generator based on this design was constructed and attached to a high voltage source at 5 kV and it produced ozone. The anode and cathode will be made out of conducting metal and will be machined to fit closely with their glass insulators. The end caps will be machined from ceramic and have an angled inlet that induces a spiral flow through the chamber maximizing the time spent in the electric field in order to increase the ozone production.

Particle Beam Inlet System

The aim of this project is to design a system for real time detection of individual airborne biological particles using laser based techniques. The work done so far involves the construction, optimization, and theoretical characterization of a particle analyzer.

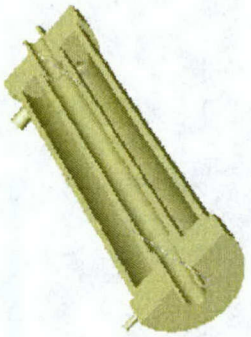

Figure 3. Cutaway of Ozone generator

Variable orifice inlet system design

One of the major problems hindering the application of laser spectroscopy in this single particle analysis scheme is the spatial misalignment between the well-confined focused laser beam waist and the incoming dispersed, low concentration flow of particles. This problem can be overcome by using an aerodynamic focusing inlet which consists of a series of concentric lenses with

Figure 4a. Particle Inlet

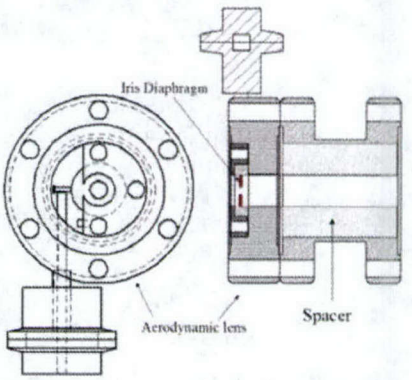

Figure 4b. Section Views of single lens lenslenseserodynmaic Lense

successively smaller orifices. This inlet system has the ability to confine particles within a certain

size range along the central axis, therefore increasing the probability of hitting the particles with the tightly focused laser beam.

Our aerodynamic inlet has two special features (Figure 4a). First, a core element of each lens is a stainless steel iris diaphragm, whose aperture can be altered from 0.8 mm to 12 mm by a mechanical linear motion feedthrough. This variable-orifice inlet system allows us to select the particle focusing size range by using different combination of lens diameters. Second, a module design makes it easy to assemble and cleanup. In addition, the geometry and the number of the lenses can be easily changed with little mechanical modification.

Numerical simulation

The focusing characteristics of the aerodynamic inlet system was modeled by FLUENT, a computational fluid dynamics (CFD) solver for numerical simulation of incompressible or compressible flows. Numerical simulation of single lens performance shows that the particle focusing dynamics relies mostly on the lens geometry (*e.g.* Lens thickness l_d, Inner tube diameter D, Lens diameter d_i), flow field properties (Reynolds number Re_f, Mach number M) and particle properties (Knudsen number K_n, Stoke number Stk). For a given inlet system, ultimately, the only adjustable variables are lens diameter and working pressure. Figure 5 shows that the particle detection efficiency, which is defined as the fraction of the injected particles entering a 500 μm detection slice placed 6.5 cm downstream of the lens, strongly depends on the lens diameter. For a given lens diameter, only particles with a specific size (optimum particle size) can be transmitted with highest efficiency. The result also implies that the variable acronymic lenses system can cover a wider particle size range under continuum regime since the optimum particle size is directly proportional to the third power of the lens diameter. Finally, the theoretical simulation also reveals that the particle detection efficiency is affected by the source pressure as well as number of lenses.

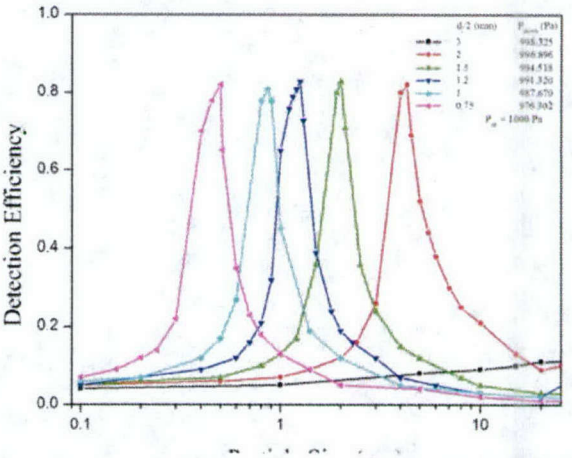

Figure 5. Effect of lens diameter(d_i) on particle detection efficiency, Re=36.3, P_{up} = 1000 Pa, tube diameter D = 12 mm, 500μm detection slice 6.5 cm downstream of the lens

Summary

To date we have done the following:

- Investigated reference materials which were used in the approach and design of the detector system.
- Selected the reactions to use for NO_2 detection.
- Designed a fully enclosed light tight reaction cell with mounting to cooled photomultiplier tube
- Selected construction materials for the detector cell
- Designed a high output electric field ozone generator
- Built a test device based on the above design, and noted ozone production.

- Selected materials for ozone generator.
- Purchased the high voltage source for ozone generator
- Selected photomultiplier tubes appropriate for given wavelength and nature of emission
- Selected explosive simulates to be used for photofragmentation studies.
- Purchased needed equipment and supplies for next stage of work.
- Built the detector cell.
- Built the ozone generator.
- Determined optimum cell design for detection for both luminal and ozone reactions.
- Determined optimum flow rates for detection.
- Developed a particle inlet system with optimized transmission efficiency.

Publications
None. Two in preparation.

Presentations
Portable Chemical Detector Kickoff Meeting, University of Montana, Missoula, MT, July 24, 2003.

Graduate Students
Pam Monterola
Ron Whiddon
Xihong Wu

Portable Chemical Agent Detection System

Annual Report
International Technology Center

During the first year of the Portable Chemical Agent Detection System project, the International Technology Center (ITC) designed and built two of the portable chemical agent detection systems that are under investigation by other members of the project team. The first system was based on photoluminescence (PL) of adsorbed vapor on constantly replenished absorbent surfaces, and the second was based on chemiluminescence of ozone-based oxidation of photofragmented explosive materials. The first generation instruments of both systems have been completed and are being tested to determine the level of performance. A second design phase has begun to further reduce the size and weight of the systems.

Photoluminescent detection of vapor from explosives is based upon the approach proposed by the University of Florida, Department of Materials Science. The prototype system designed and constructed at ITC makes use of a green diode laser as the excitation source. The sample collection method makes use of a 15cfm collection fan that directs the vapor at a roll of paper tape, a method commonly used by MDA and others as a basis for chemical analysis of hazardous gases. The flow was maximized as much as possible in the initial stages, to reduce the collection time needed for the expected low concentrations of explosive vapor. The luminescent beam was then chopped to provide a basis for measuring changes in the intensity as a function of exposure. The detector used for the PL apparatus was initially a solid state detector from an Ocean Optics HR2000 spectraphotometer. The detection scheme utilized in the final prototype was a narrow bandpass filter in combination with a cooled photomultiplier tube (PMT) from Hamamatsu. A laptop computer was utilized to collect and store the data. The instrument was enclosed in a black ABS plastic box and had a total weight of approximately 14lbs. The total size of the analysis system was $1ft^3$, $0.3ft^3$ for the data acquisition system, and $0.3ft^3$ for the laptop with a total weight of 23lbs. The results of the spectral analysis with 1000ppm standard solutions of TNT, either from adsorbed vapors or crystallized TNT on Si or Gold substrates showed no PL peaks at the 705nm wavelength that was originally associated with TNT by the University of Florida.

The second system was modeled after a design proposed by the University of Florida, Department of Chemistry. The system for explosive vapor detection was based on photofragmentation of collected gas vapor followed by a reaction with a luminescent medium. The explosives are predominantly nitrogen-based compounds and photofragmentation of the volatile nitrogen compounds occurs readily in the deep UV region (~266nm). This system provide close to real time analysis of the collected vapor. The system at Florida was based initially on excimer laser photofragmentation. The most portable excimer laser that we could find was still hundreds of pounds and required large amounts of power to operate. Florida's analysis concluded that photofragmentation was the best method for fragmenting the nitrogen-based compounds. Therefore, the first system designed at ITC was based upon the use of a broad-beam flashlamp-based photofragmentation system. A power supply was designed and built for a 10-100Joule, 20-40 microsecond pulse Xe flash lamp. The flashlamp provides excitation wavelengths down to 250nm. The 15cfm sample collection system was placed on a

0.25in diameter quartz tube. The tube was wound around the Xe flashlamp and contained inside a stainless steel sleeve. The stainless was insulated from the flashlamp chamber with fiberglass insulation because the heat of operation made the stainless too hot to hold. The travel time through the tubing was selected to provide at least two flashes during transit. After the flash, the gas enters a gold-coated parabolic analysis chamber. Ozone is mixed with the photofragmented gas and in the presence of the volatile nitrogen compounds, forms a more stable nitrogen oxide with the emission of an IR photon in the range of 800-1200nm. The photons are focused toward the end of the parabolic chamber where a PMT with an IR filter counts the photons produced.

There are two difficulties with this mode of operation. The first is the photofragmentation, which was done outside the analysis chamber and may have undergone recombination in the gas stream before entering the chamber. This situation was necessary since the flashlamp could not be incorporated into the parabolic chamber due to temperature concerns. The most important difficulty was the weight and size of the power supply. The power supply alone weights ~85lbs, which although an improvement over an excimer laser, was hardly portable. A 40 lbs lighter switch-mode power supply was designed and tested, but did not produce sufficient current and rise time. ITC then undertook a lighter and lower power design which utilized a ND-YAG Q-switched laser at 266nm. The laser produces a 1μj - 10μs pulse at a maximum pulse repetition frequency of 10kHz. The results are currently being evaluated. However, the system weight is now approximately 29lbs with a total volume of $1ft^3$.

The on-going effort is aimed at further reductions of size and weight of the chemiluminescence-based instrument and to quantify the data collected using the new laser-based detection system. The further reductions in size and weight will be accomplished with the removal of the laptop computer and migration of the analysis software to a handheld device.

Final Report

Pacific Northwest National Laboratory
Real-Time Optical Probes Based Upon Inelastic Light Scattering

OBJECTIVE

The objective of this research is to develop a portable probe for real-time detection of chemical agents based on Raman spectroscopy that also makes use of signal enhancement strategies such as Surface Enhanced Raman Spectroscopy (SERS) and the incorporation of novel high-surface-area substrates based upon ultra-porous mineralized wood.

SUMMARY OF KEY ACCOMPLISHMENTS

- Fabrication of mineralized wood samples for substrates.
- Characterization of optical properties of substrates and quantification of fluorescence emission from substrates as a function of wavelength.
- Purchase of new, back-illuminated, deep-depletion, CCD detector for Raman studies. This detector will permit sensitive Raman studies at 900 nm and greater, where fluorescence interference is minimal. Delivery is expected shortly. (Funds for purchase of this equipment were leveraged from a different program.)
- Quantification of SERS effect on mineralized wood substrates as a function of wavelength.
- Quantification of surface-area effects from mineralized wood substrates.
- Preliminary identification of the mechanism of adsorption of organics on mineralized wood substrates.

DISCUSSION

Although it has high chemical specificity, the Raman effect is typically a weak effect with signal intensities below those required for detecting trace amounts of chemicals in real-world environments. However, several approaches have been shown to enhance Raman signals, in some cases by several orders of magnitude. This work focuses on evaluating a combination of two of these approaches: use of high-surface-area substrates and SERS. The goal of this part of the project is to develop a sensitive Raman probe that could be integrated with an optical fiber to enhance sensitivity of the Raman method. The impetus for pursuing this approach is based upon the physiology of the nose where the sensor organ itself has a high surface area reminiscent of the structure of wood.

Recent work in our lab successfully synthesized samples of mineralized wood with nano-scale architectures and extremely high surface area. Because of this high surface area, the materials were deemed to be promising for use as substrates for Raman spectroscopy and were proposed for further study in the current project. The use of SERS was also evaluated in conjunction with the high-surface-area samples. In SERS, nano-scale particles of Au or Ag were deposited on the mineralized wood substrates. Interactions between the incident laser beam and the metal particles results in an enhancement of the excitation signal, which, in turn, typically produces a pronounced increase in Raman intensities.

Mineralized pine samples were coated with Au or Ag particles (for the SERS effect) using different procedures and different amounts of the noble metals. The samples were then exposed to pyridine vapors. Raman spectra of these samples were obtained and the intensities of the pyridine peaks were measured. Pyridine was selected as a trial molecule for two reasons: (1) it has been a standard molecule for evaluating the SERS effect; and (2), the heterocyclic ring structure is indigenous to toxic nerve agents. The Raman intensities were considered indicative of the extent to which the approach could be used to detect organic molecules with similar functionality that were present in the gas phase, as would be the case in environments where a chemical agent probe might be deployed.

Figure 1 shows the Raman spectra of a mineralized pine sample with different types of SERS-pretreatment (i.e. Au or Ag) and excitation at 514.5 nm (green). Figure 2 shows similar spectra with excitation at 778.7 nm (near IR). As shown, the substrate fluoresces significantly in the green, but not nearly as much at longer wavelengths. Measurements at 488 nm indicated even more fluorescence in the blue. For excitation at 514.5 nm, the SERS effect made it possible to observe the pyridine peaks near 1000 cm^{-1}, with the sensitivity depending somewhat on the metal-particle pretreatment procedure. However, the relative intensity of the Raman peaks and fluorescence background, even with SERS, was still unsatisfactory because the fluorescence background was so large. At 778.7 nm, the fluorescence background was much smaller and the pyridine peaks more easily observed. Surprisingly, the most intense pyridine peaks were observed when no SERS pretreatment procedures were used (no Au or Ag). This indicates that the SERS effect (using Au or Ag) may be weak with 778.7 nm excitation, the metal particle morphology has not been tailored appropriately, or that there are other reasons why the pyridine peaks are so large and that the *relative* effect of SERS is markedly less.

Fig. 1. Pyridine on Pine at 514.5 nm

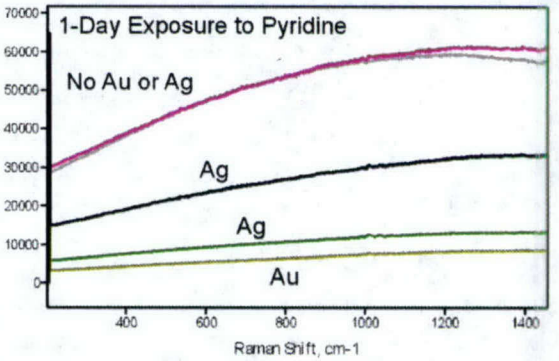

Fig. 2. Pyridine on Pine at 778.7 nm

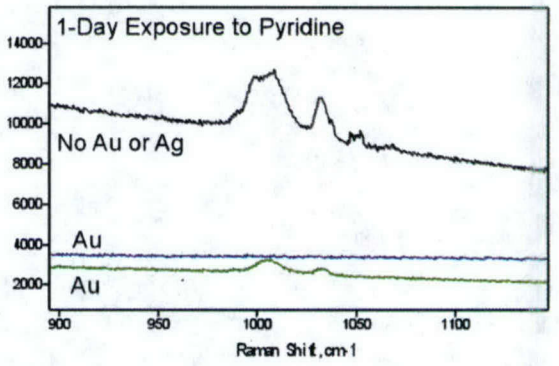

At this time, we suspect that the reason for the strong pyridine peaks is the high surface area of the substrates and the strong tendency of organic molecules to adsorb on them. Figure 3 shows that the organics can be removed with heating. Interestingly, the desorption process appears to occur in two steps. A sample of mineralized pine exposed to pyridine vapors exhibits Raman peaks at the same frequencies as neat pyridine, i.e. 991 and 1031 cm^{-1}, as well as broader peaks

shifted to slightly longer wavelengths, i.e. 1008 cm^{-1} and 1035 cm^{-1}. We believe that the latter arise from pyridine molecules adsorbed directly on the surface, while the peaks resembling the neat sample arise from an outer, condensed, layer of pyridine liquid. Heating the sample at 93°C results in a loss of the outer layer without affecting the adsorbed layer significantly. The adsorbed layer is removed at approximately 165°C, as shown in Figure 4.

Fig. 3. Effect of Heating on Pyridine on Pine

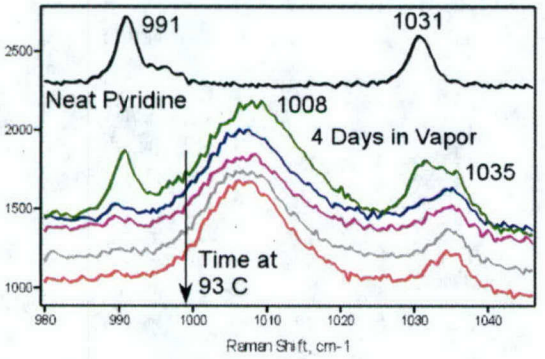

Fig. 4. Effect of Heating on Pyridine on Pine